Temperature Effect on NMR Surface Relaxation in Rocks for Well Logging Applications

S. Godefroy,[†,‡] M. Fleury,[†] F. Deflandre,[†] and J.-P. Korb*[,‡]

Institut Français du Pétrole, 92852 Rueil-Malmaison, France, and Laboratoire de Physique de la Matière Condensée, UMR 7643 du CNRS, Ecole Polytechnique, 91128 Palaiseau, France

Received: June 5, 2002

We present nuclear spin-relaxation experiments, at various temperatures and Larmor frequencies for water and oil confined in a series of calibrated porous media and various natural rocks. The temperature and frequency dependencies of the longitudinal nuclear spin relaxation rates $1/T_1$ are interpreted with an original model of surface diffusion taking into account the solid−liquid interactions with the pore surface. Depending of the strength of such interactions, one observes an anomalous temperature dependence of the transverse $1/T_2$ and longitudinal $1/T_1$ nuclear spin-relaxation rates for water in silica and various sandstones and a normal temperature behavior for water-saturated calcium carbonate surfaces. The model supports also the normal temperature dependence observed for oil saturated porous media at proximity of silica, sandstone, and carbonate surfaces. The potential impact of this study for NMR well logging applications is also discussed.

I. Introduction

Nuclear magnetic resonance (NMR) well logging is now routinely used to determine the fundamental properties of reservoir rocks, such as porosity, pore size distribution, and saturation.[1,2] From the pore size distribution, an estimation of the permeability can also be deduced. It is known that reliable, in-situ nuclear spin relaxation measurements must be calibrated with laboratory experiments performed on core plugs. However, the laboratory data are usually collected at room temperature, whereas reservoir temperatures can be as high as 150 °C. The temperature dependence of the nuclear spin-relaxation rates should thus be considered. For bulk liquids, one generally observes a normal temperature behavior of these rates due to a pure diffusive dynamics. For confined liquids where the relaxation is dominated by the interactions with the surface, the temperature dependence is unclear because a fine understanding of the liquid−solid interaction is generally not available. Previous experiments of the temperature dependence of NMR relaxation of water in natural rocks, with a broad pore size distribution, have shown a weak and negligible effect.[3] In a recent publication, we showed by using field cycling nuclear magnetic relaxation technique on calibrated porous media, an anomalous temperature dependence of the nuclear spin-relaxation rates, depending on the liquid−solid interaction at the pore surface. Here, we consider again such a temperature effect but on grain packings of different mineralogy as well as natural rocks (from outcrop and oil reservoirs) of different wettability.

Basically, the standard NMR relaxation experiments in porous media consist in the measurement (in-situ or in the laboratory) of the transverse, $1/T_2$, relaxation rates of the liquids (water and oil) saturating the samples. In the case of in situ NMR measurements during drilling, the longitudinal, $1/T_1$, relaxation rates are preferred for various technical reasons. For each fluid present in the porous space, the biphasic fast exchange model between the molecules within the pores and transient surface molecules occurs, and these two rates are directly related to the surface-to-volume ratio (S/V) of the pore by

$$\frac{1}{T_{1,2}} = \frac{1}{T_{1,2\mathrm{B}}} + \rho_{1,2}\frac{S}{V} \tag{1}$$

Here, $1/T_{1\mathrm{B}}$ and $1/T_{2\mathrm{B}}$ are the longitudinal and transverse bulk relaxation rates, respectively. ρ_1 and ρ_2 are the longitudinal and transverse surface relaxivity parameters, respectively. These two overall rates, $1/T_1$ and $1/T_2$, are measured by usual NMR radio frequency pulse sequences.[5] When both oil and water are present in the porous space, the wettability plays a role, and both water and oil molecules can interact with the surface. The surface relaxivity parameters ρ_1 and ρ_2 depend on both the surface and liquid characteristics, and an important literature can be found concerning water surface relaxivity on various surfaces.[1,6] For petroleum applications, the relaxivity of oil must also be considered because of the existence of oil-wet surfaces in many reservoir rocks.[7] Therefore, both water and oil relaxation times can be dominated by surface interactions and potentially depend on temperature.

In this paper, we first outline our theoretical model of frequency and temperature dependence of surface relaxivity $\rho_{1,2}$ in porous media.[4] The temperature dependence of the relaxation rates obtained on water or oil (dodecane) saturated calibrated grain packings support our theory. Finally, we present similar experiments performed on natural (outcrop and reservoir) rocks, which exhibit the similar expected temperature dependence. We finally discuss the potential impact of this study for well logging applications.

II. Theoretical Background and Experiments on Model Porous Media

1. Frequency and Temperature Dependence of Surface Relaxivity. We consider a large number of protons (I) spin-bearing molecules (water or oil) diffusing in pores with a surface density σ_S of fixed paramagnetic impurities of spins (S; Figure 1). With the gyromagnetic ratio of the electron, γ_S, being much

* To whom correspondence should be addressed. Fax 33 1 69 33 30 04. E-mail: jean-pierre.korb@polytechnique.fr.
† Institut Français du Pétrole.
‡ Ecole Polytechnique.

10.1021/jp0213452 CCC: $22.00
Published on Web 10/09/2002

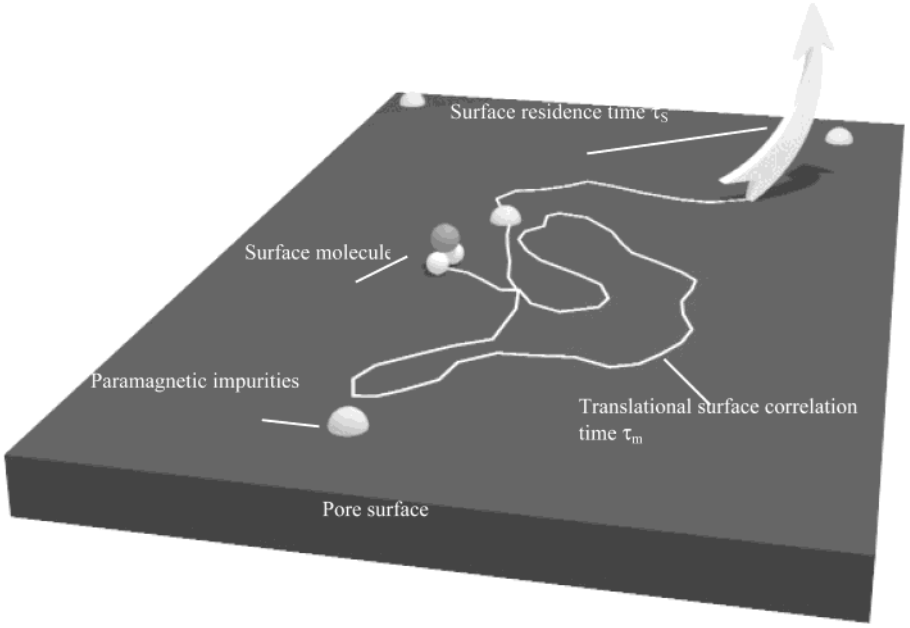

Figure 1. Model of the two-dimensional translational diffusion of the proton species at the pore surface. The spin-bearing molecules (for example, water) diffuse at the surface, sometimes reaching fixed surface paramagnetic impurities where the spins relax. The translational surface correlation time is defined as τ_m. This surface motion is interrupted by the surface desorption, characterized by a surface residence time τ_S.

larger than that of the proton, γ_I, ($\gamma_S = 658.21\gamma_I$), the proton spin relaxation is thus due to the modulation of the dipole−dipole interactions between I and S spins by translational diffusion.[5,8] The situation has been well documented for the case of bulk liquids[5] and general statements have been proposed for the case of porous media.[1,6,9] However, the confinement effect that occurs in porous media as well as the surface diffusion of liquids requires another theoretical approach. This is particularly important at low magnetic field in NMR well logging applications, where the surface molecular dynamics is probed on a much wider time scale. We have recently addressed this problem on the basis of the following considerations.[4]

(i) The biphasic fast exchange between surface and bulk molecules, even in macroporous media where the surface-to-volume ratio S/V is very small, enhances drastically the surface contribution in eq 1 especially at low frequency.

(ii) The main contribution of the proton relaxation comes from the two-dimensional motion of the molecules at the pore surface near the fixed relaxing sinks S.

(iii) The numerous two-dimensional $I-S$ molecular reencounters are responsible for the net frequency dependence observed for the longitudinal spin-relaxation rates.

(iv) The residence time of the studied liquid at the pore surface depends on the existence of potential chemical bonds with specific surface groups.

(v) We introduce two correlation times in the theory. The translational correlation time, defined as τ_m, is associated to individual molecular jumps at the surface. The surface residence time, defined as τ_s, is limited by molecular desorption. A schematic description of the molecular surface motion is presented on Figure 1. All of these considerations lead, after some calculations detailed in refs 4, 10, and 11, to the following logarithmic expression of the longitudinal surface relaxavity at low frequency:

$$\rho_1(\omega_I,T) = \alpha\tau_m \ln\frac{1+\omega_I^2\tau_m^2}{(\tau_m/\tau_S)^2+\omega_I^2\tau_m^2}$$

with

$$\alpha = \frac{N_S}{N}\frac{\pi}{20}\frac{\sigma_S}{\delta^4}(\gamma_I\gamma_S\hbar)^2 S(S+1) \qquad (2a,b)$$

Here N_S/N is the ratio of number of liquid molecules at the surface and in the volume, respectively. σ_S is the surface density of paramagnetic impurities, and δ is the distance of minimal approach between I and S spins. Such a logarithmic frequency dependence has been experimentally evidenced in calibrated porous media by using the field cycling NMR method.[4] In the following, we focus on the temperature dependence of the surface relaxivity, which comes directly from the Arrhenius laws for the correlation times:

$$\tau_m(T) = \tau_{m0}\exp\left(\frac{\Delta E}{RT}\right) \qquad (3)$$

where $\Delta E = E_m - E_s$ is an effective activation energy describing the surface translational motion, R is the gas constant, and T is the temperature. E_m is the usual activation energy associated to the individual molecular diffusing jumps. For instance, $E_m \approx$ 4.8 kcal/mol for bulk water. E_s is the activation energy associated to the surface interaction. When the diffusing barrier is larger than the surface interaction, namely, when $\Delta E > 0$, one expects a normal temperature dependence of the surface relaxivity; that is, ρ_1 decreases when the temperature T increases. On the contrary, when $\Delta E < 0$, one expects an anomalous temperature dependence where ρ_1 increases with the temperature. For the transverse surface relaxivity ρ_2, the expected temperature dependence is similar to the one described above and proportional to the translational correlation time

$$\rho_2(T) \propto \alpha\tau_m(T) \qquad (4)$$

but the frequency dependence of ρ_2 is much weaker than that of ρ_1.

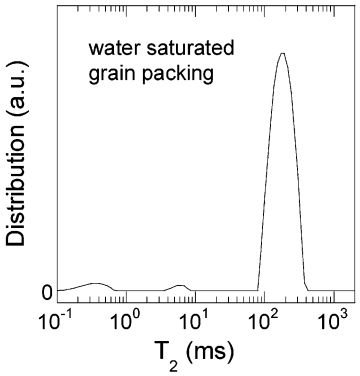

Figure 2. Distribution of relaxation times T_2 of a packing of silicon carbide grains of 8 μm of diameter, saturated with water.

III. Experimental Validation on Model Calibrated Porous Media

1. Methods. The frequency dependence of the longitudinal relaxation rates, $1/T_1$, measured on different systems gives a strong experimental support of eq 2 and is described in detail in a previous publication.[4] Here, we focus on the temperature dependence and present experiments performed on three different instruments. We have used a magnetic field cycling instrument of the Redfield design,[12] to measure $1/T_1$ for frequencies varying in the range 0.01−20 MHz, at different temperatures. The experiments were performed on a homemade field cycling instrument at the department of Chemistry of the University of Virginia (laboratory of R. G. Bryant, Charlottesville) and on a fast field cycling, Stelar instrument (Italy) at LPMC, Ecole Polytechnique (France). We measured the transverse relaxation times, T_2, at 2.2 MHz on a Resonance Instrument (England) Maran-2 spectrometer, using a standard spin−echo CPMG sequence,[5] at IFP (France). The magnetization decay curves were analyzed in term of relaxation time distributions using a multiexponential decomposition process in which an optimum regularization term is calculated based on Butler et al.'s method.[13] For narrow distributions of relaxation times, the data were also analyzed by using a simple exponential fit to determine the mean relaxation times, therefore increasing the accuracy of the measurements. The variation of T_2 as a function of the temperature was obtained by using a special cell described in the Appendix, allowing temperature measurements from 10 up to 100 °C with an accuracy of ±1 °C.

The different samples were selected mainly for their narrow pore size distributions, allowing a much easier study of the temperature effect than in porous media with broad pore size distribution, where the temperature effect can be influenced by the pore coupling. The samples were saturated either with water or oil (dodecane) using vacuum line techniques.

2. Materials. The first kind of samples consists of a series of packings of grains calibrated in size. Nonporous silicon carbide, SiC, grains (from Peter Wolters, Germany) were packed using different calibrated grain of characteristic size in the range 8−150 μm. The packing procedure provided a series of calibrated porous media with pore sizes approximately the same as the grain sizes and with a porosity of about 45%. X-ray photoelectron spectroscopy (XPS)[14] has shown that SiO_2 covers 25% of the grain surface, representing hydrophilic zones. The narrow pore size distribution is evidenced by the observed narrow transverse relaxation times (T_2) distribution, as presented on Figure 2 for the water saturated 8 μm grain packing. Because of the grain preparation, the surfaces contain paramagnetic impurities that originate either from the grinding process or derived from the silicon carbide synthesis. We removed the grinding impurities by applying a continuous flux of hydrochloric acid through the porous media for a few weeks. Electron spin resonance (ESR) experiments performed on the dry grains after cleaning showed that ferric ions (Fe^{3+}) still remained in the grains.

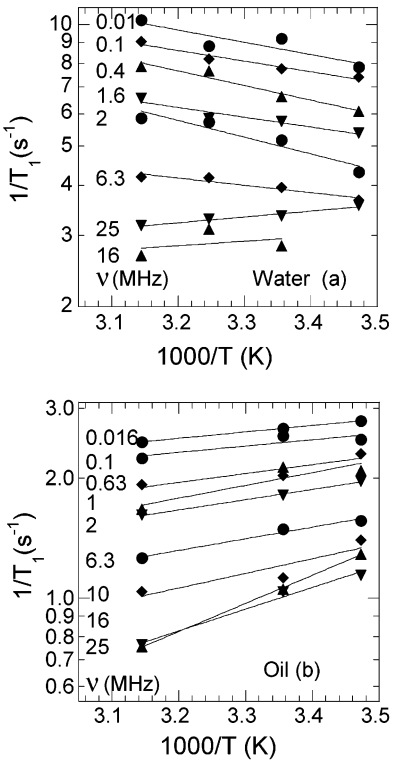

Figure 3. Arrhenius diagrams of the measured relaxation rates of liquids saturating the 8 μm grain packing, as a function of the inverse of temperature, 1000/*T*, for different proton Larmor frequencies, ν, (a) for water and (b) for oil.

The second kind of sample is a packing of calcite ($CaCO_3$) grains. These grains (Mikhart SPL, from Provencale, France) have an analytical grade of 99.1%. The largest grain diameter is 50 μm, with a mean diameter of 20 μm. We measured a porosity of 43% for the granular packing. The presence of Mn^{2+} paramagnetic ions has been evidenced by ESR from its typical hyperfine structure.

3. Results. We display on Figure 3 parts a and b the temperature dependence of $1/T_1$, at different frequencies, for the 100% water or 100% oil saturated 8 μm grain packing. The temperature dependence of $1/T_1$ for water below 10 MHz (Figure 3a) is inverse to that obtained in all other situations: oil saturated packing (Figure 3b), water saturated packing above 10 MHz, and bulk water. As described in the theoretical section, this unusual situation where $1/T_1$ increases with the temperature is due to the hydrogen bonds of water with the numerous silanol groups at the silica pore surface. In fact, the low and negative value of the measured effective activation energy $\Delta E \approx -2$ kcal/mol, obtained from the slopes of the curves in Figure 3a at low frequency, is representative of the proton exchange occurring at the pore surface between the silanol groups and the first hydration shell of water.[4] When taking $E_m = 4.8$ kcal/mol, one can deduce an activation energy E_s of 6.8 kcal/mol, a value also found in nanoporous silica glasses.[10,11] For oil (dodecane), the measured mean activation energy on the surface, about +2 kcal/mol, is much closer than that of bulk oil (measured value +2.6 kcal/mol). Here, we observe a normal

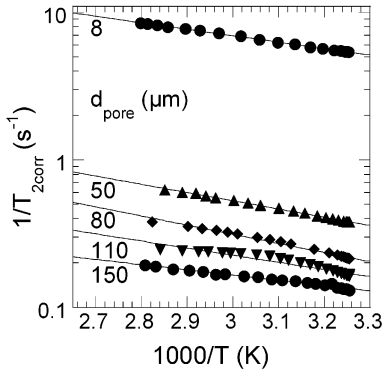

Figure 4. Arrhenius plot of the variation of the mean transverse relaxation rates, $1/T_2$, as a function of the inverse of the temperature, $1000/T$, of water saturating the packing of different grain size, varying in the series {8, 50, 80, 110, and 150 μm}. The measured temperature variation is opposed to the water one's. One measures an activated energy $\Delta E \approx -2$ kcal/mol.

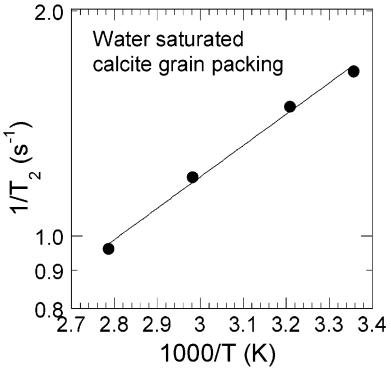

Figure 5. Arrhenius diagram of the variation of the measured transverse relaxation rate, $1/T_2$, as a function of the inverse of the temperature, $1000/T$, of water saturating the calcite grain packing. One measures an effective activation energy of 1.9 kcal/mol.

temperature behavior of the relaxation rate, which indicates a pure diffusive dynamical process.

In complement, we have measured the temperature dependence of the proton transverse relaxation rates, $1/T_2$, of the water saturated grain packs for the different pore sizes (ranging from 8 to 150 μm; Figure 4). To emphasize the anomalous temperature dependence of the surface contribution of $1/T_2$, we have corrected the measured relaxation rates from the bulk contribution according to

$$\frac{1}{T_{2\mathrm{corr}}} = \frac{1}{T_2} - \frac{1}{T_{2\mathrm{B}}} \tag{5}$$

The results obtained confirm the observed anomalous temperature dependence obtained for $1/T_1$. In particular, we find the same activation energy $\Delta E \approx -2$ kcal/mol. More generally, these results prove again the anomalous temperature dependence of ρ_2 for water on silica surfaces, as described in the theoretical section.

The temperature behavior depends on the activation energy E_s of the surface chemical bonding, and therefore, the physical chemistry at the liquid−solid interface is of particular importance. For instance, for calcite, one observes a normal temperature dependence of $1/T_2$ for water saturated grain packing of calcite (Figure 5), with an effective positive activation energy of $\Delta E \approx 1.9$ kcal/mol.

IV. Temperature Experiments on Natural Porous Rocks

In the following, we apply the method described above on sandstone and carbonate rocks, either from outcrop or oil reservoir. They were saturated either with water or oil to obtain the water or oil surface relaxivity temperature dependence. From the point of view of this study, the pore surface of reservoir samples differ from that of outcrop samples in the presence of adsorbed oil components (e.g., polar components), changing their wettability and the liquid−solid interactions. We will see that the trends observed on model porous media are still valid, despite the complexity of natural rocks.

The samples were selected for the absence or very low clay content (particularly for the sandstones) and for their narrow pore size distribution. Therefore, the temperature effect can be associated to surface relaxivity and not to pore coupling. The outcrop rocks are water-wet, and the reservoir ones are of intermediate wettability.

1. Core Samples. *Sandstone Rocks.* The outcrop sandstone studied is a Clashash sandstone of porosity 17% and water permeability of about 500 mD. The mercury porosimetry shows that the pore throat radius distribution is narrow. The clay content is very small, as shown by T_2 relaxation time distribution measurements.

The reservoir sandstone studied has a porosity of 19% and a water permeability of 840 mD. Electronic microscopy has shown that the rock is composed of quartz grain of diameter varying from 30 to 500 μm, sometimes cemented by carbonate. One notes that some of the pores are filled with clays (principally kaolinite). However, the clay-bound water volume measured by NMR represents no more than 2% of the total porosity. The mercury porosimetry shows that the pore throat radius distribution is very narrow and peaks at 14 μm. The sample has been cleaned using various solvents according to IFP's standard procedure in order to avoid any contamination of the samples during coring in the well. Then, they were aged in reservoir crude oil for 3 weeks at the reservoir temperature[7] to reproduce in-situ wettability conditions occurring in the reservoir. The USBM wettability test[15] (based on measurements of capillary pressure) performed after aging indicates a wettability index of -0.19, indicating that oil is in contact with the pore surface in the presence of water.

Carbonates. The outcrop carbonate used is a fine grain Lavoux limestone of porosity 23% and of water permeability around 3 mD. This limestone rock is typical of a water-wet $CaCO_3$ surface. The narrow pore size distribution of the rock is evidenced by the narrow T_2 distribution of the water saturated sample measured at 2.2 MHz.[4] Mercury porosimetry experiments indicate a mean pore throat radius of 0.5 μm. ESR measurements performed on this rock have shown the presence of Mn^{2+} paramagnetic impurities.

The reservoir carbonate sample studied has a porosity of 24% and a water permeability of 1.5 mD. Electronic microscopy of this rock exhibits the presence of crystals of $CaCO_3$ varying in size from 1 to 20 μm. From mercury porosimetry, the pore throat radius distribution is narrow and peaks at 0.5 μm. ESR experiments have evidenced the presence of Mn^{2+} paramagnetic ions. The sample has been cleaned according to IFP's standard procedure.[7] The USBM wettability test performed after cleaning indicates a wettability index of $+0.50$. During the wettability test, a spontaneous imbibition of water was observed but the cleaning procedure was not sufficient to remove some absorbed components from the surface, resulting in a nonstrongly water-wet state.

2. Results. We analyze in this section a series of experimental data that prove that the concepts introduced above for model porous media can be extended to describe the temperature

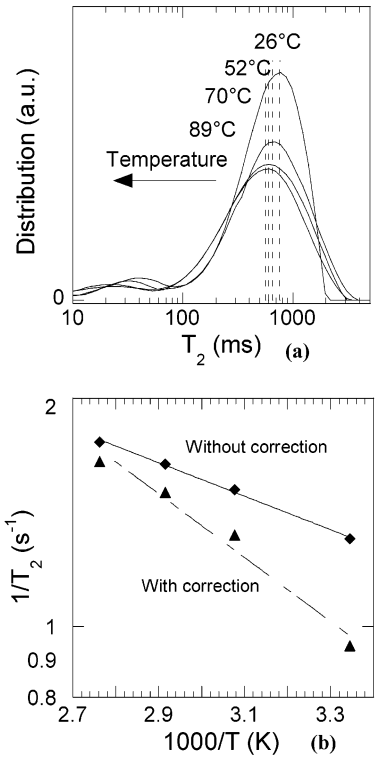

Figure 6. (a) Variation of the transverse relaxation time distribution, T_2, as a function of the temperature, of water saturating a Clashash sandstone. One notes that T_2 decreases with increasing temperature. **(**b**)** Arrhenius plot of the variation of the mean measured, $1/T_2$, (◆) and corrected from the bulk contribution (eq 5), $1/T_{2corr}$, (▲) transverse relaxation rates as a function of the inverse of the temperature, 1000/*T*, of water saturating a Clashash sandstone. One notes a temperature variation in opposition to the bulk water one's, with a measured effective activation energy of −2 kcal/mol.

TABLE 1: Variation of T_2 of Water Saturating the Clashash Sandstone

temp °C	T_2 peak (ms)	T_{2corr} (ms)
26	800	1137
52	670	779
70	600	656
89	565	600

dependence of the relaxation rates of water and oil in natural rocks.

Sandstone Rocks. For the Clashash outcrop sandstone fully-saturated with water, the variation of the transverse relaxation time distributions, T_2, measured at 2.2 MHz as a function of the temperature is presented in Figure 6a. The general tendency is an anomalous temperature behavior where the relaxation times decrease when the temperature increases. Figure 6b presents the temperature dependence of the central peak (given in Table 1) of the distribution of $1/T_2$ described in Figure 6a. From the Arrhenius diagram of the corrected values (eq 5), we find an effective activation energy $\Delta E \approx -2$ kcal/mol. This result is confirmed from the variation of $1/T_1$ of water in this rock as a function of the temperature and for different frequencies, obtained by the field cycling technique and displayed in Figure 7.

For the reservoir sandstone moderately oil-wet (Iw = −0.19) and fully saturated with water, the transverse relaxation time distributions are presented in Figure 8a, for different temperatures. The general tendency is also an anomalous decrease of the water relaxation times with increasing temperature but weaker than for the outcrop sandstone. The values of the peak

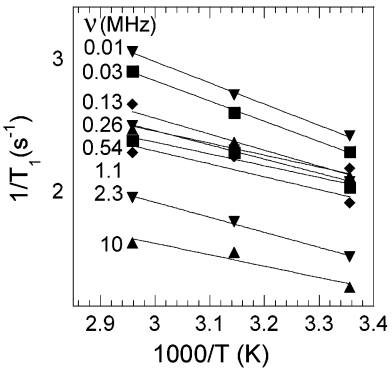

Figure 7. Arrhenius diagrams of the measured longitudinal relaxation rates, $1/T_1$, of water saturating a Clashash sandstone, as a function of the inverse of temperature, 1000/*T*, and for different Larmor frequencies ν.

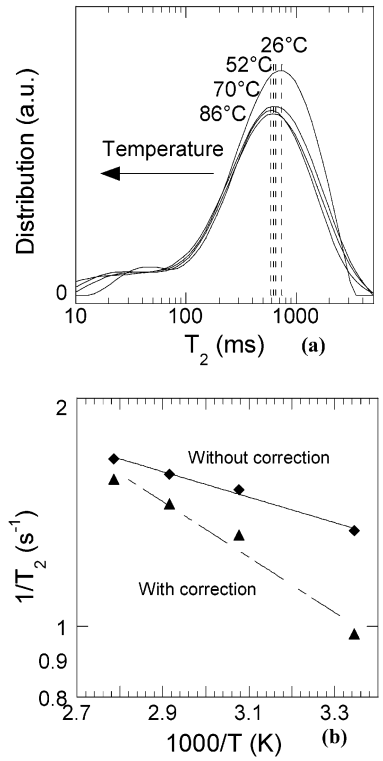

Figure 8. (a) Variation of the transverse relaxation time distribution, T_2, as a function of the temperature, of water saturating a reservoir sandstone. One notes that T_2 decreases with increasing temperature. **(**b**)** Arrhenius plot of the variation of the mean measured, $1/T_2$, (◆) and corrected from the bulk contribution (eq 5), $1/T_{2corr}$, (▲) transverse relaxation rates, as a function of the inverse of the temperature, 1000/*T*, of water saturating the reservoir sandstone. One notes a temperature variation in opposition to the bulk water one's, with a measured effective activation energy of −1.7 kcal/mol.

TABLE 2: Variation of T_2 of Water Saturating the Reservoir Sandstone

temp °C	T_2 peak (ms)	T_{2corr} (ms)
26	710	963
52	660	765
70	620	680
86	595	633

relaxation times corresponding to the distributions of Figure 8a are given in Table 2. Figure 8b shows the Arrhenius diagram of $1/T_2$ of water in this sandstone. When corrected for the bulk values (eq 5), one finds an effective activation energy of $\Delta E \approx -1.7$ kcal/mol.

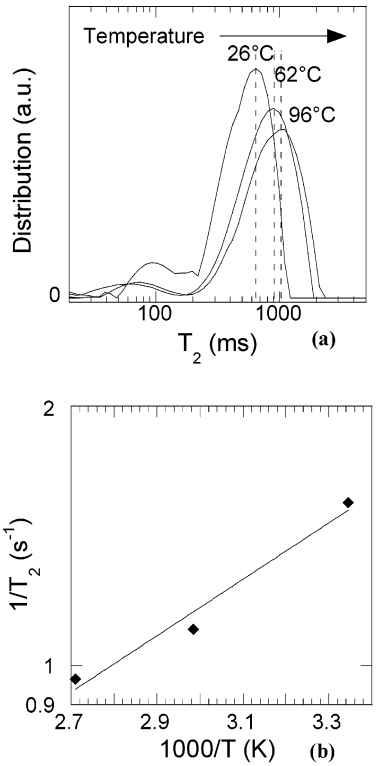

Figure 9. (a) Variation of the transverse relaxation time distribution, T_2, as a function of the temperature and of oil (dodecane) saturating a reservoir sandstone moderately oil wet (Iw = −0.19). One notes that T_2 increases with increasing temperature. **(b)** Arrhenius plot of the variation of the mean measured transverse relaxation rates, $1/T_2$, as a function of the inverse of the temperature, $1000/T$, of water saturating the reservoir sandstone.

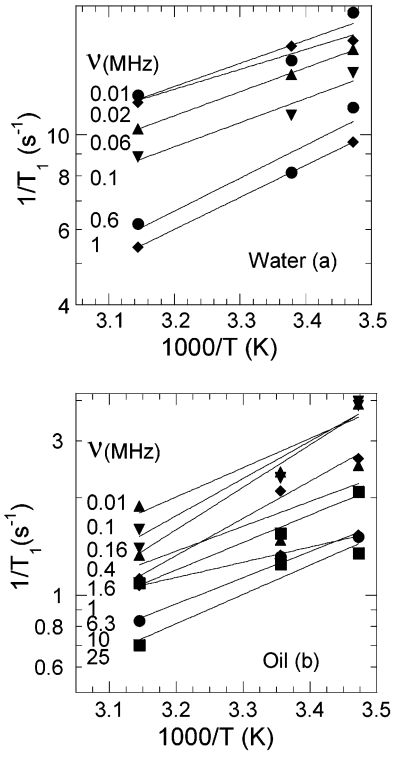

Figure 10. Arrhenius diagrams of the measured relaxation rates of liquids saturating a limestone rock (Lavoux), as a function of the inverse of temperature, $1000/T$, for different proton Larmor frequencies, ν, (a) for water and (b) for oil.

For the reservoir sandstone 100% oil-saturated, the transverse relaxation time distributions, measured at 2.2 MHz and for different temperatures, are shown in Figure 9a. One observes a normal temperature dependence of $1/T_2$, corresponding to the relaxation times of the peaks of the distributions. On this oil-wet surface, one notes that oil relaxation times are smaller than the bulk's one, indicating an efficient surface relaxivity. From the slope of the curve of Figure 9b, one obtains $\Delta E \approx 1.5$ kcal/mol.

Carbonates. We display on Figure 10 parts a and b, the normal temperature dependence of the longitudinal relaxation rates of water and oil, respectively, when saturating the core of the outcrop limestone. Both water and oil relaxation rates follow the same normal temperature dependence. For water, one measures a mean effective activation energy of +2.5 kcal/mol.

For the reservoir carbonate, we plotted in Figure 11a the temperature variation of the transverse relaxation time distribution (at 2.2 MHz) of water fully saturating the core. As for the limestone rocks, relaxation times increase with the temperature. The mean relaxation times, T_2, corresponding to the middle of the distribution peaks, are given in Table 3 for the different temperatures. The Arrhenius diagram of Figure 11b, of $1/T_2$, leads to a measured activation energy of $\Delta E \approx +1.9$ kcal/mol.

For this reservoir carbonate, the variation as a function of the temperature of the longitudinal relaxation rates, $1/T_1$, measured at different Larmor frequencies using the field cycling technique, are presented in parts a and b of Figure 12, of water and oil, respectively, saturating the core at 100%. One measures about the same activation energy for water than the one given by $1/T_2$, and an activation energy of 2.4 kcal/mol for oil.

3. Discussion and Application NMR Well Logging Calibration. From the various experiments described above, we can observe general trends describing the temperature dependence of the surface relaxivity (Table 4). For water- or oil-wet surfaces composed mainly of silica, (SiC grain packing, Clashash and reservoir sandstones), the water surface relaxivity parameters increase with temperature according to eqs 2−4, with an observed effective activation energy in the range −2 to −1.7 kcal/mol, and the oil surface relaxivity parameters decrease with temperature with an observed effective activation energy in the range 1.5−2 kcal/mol. For water-wet or weakly water-wet surfaces composed mainly of $CaCO_3$ (calcite grain packing, Lavoux limestone and reservoir carbonate), the water or oil surface relaxivity decreases with temperature with an effective activation energy in the range 1.9−2.5 kcal/mol. Note that we used a refined oil (dodecane) as the oil phase to determine the oil surface relaxivity. More complex fluids (mud oil filtrate or native crude oil) might complicate the analysis, but the general trends should still be valid.

When laboratory and log data are compared in similar saturation conditions, the relaxation times might be shifted by a factor equal to the exponential term in eq 3. For instance, from 25 °C up to 120 °C, a shift of a factor about 2.1 is possible (taking $|\Delta E| = 2$kcal/mol), either in reducing or increasing the relaxation times depending on the type of surface and the fluid considered. In practice, the temperature effect might be hindered by pore coupling when considering bimodal pore structures or by mixed surface composition (quartz and calcite). There are also further complications related to the existence of static magnetic field gradient present in the logging tools that prevent the measurements of long relaxation times.

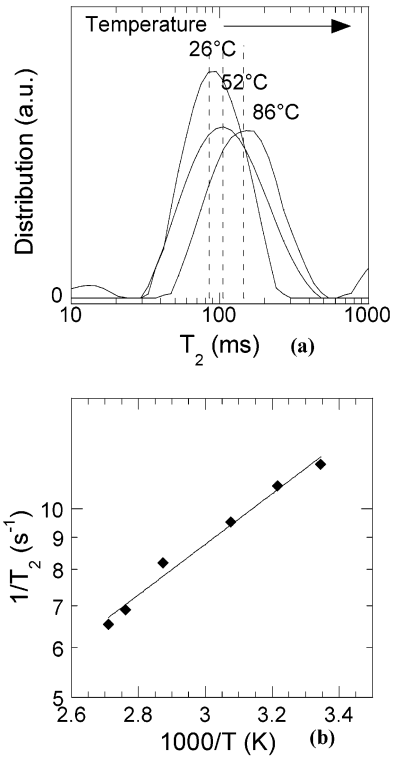

Figure 11. (a) Variation of the transverse relaxation time distribution, T_2, as a function of the temperature, on water saturating a reservoir carbonate of intermediate wettability (Iw = +0.50). **(b)** Arrhenius diagram of the variation of the mean transverse relaxation rates, $1/T_2$, as a function of the inverse of the temperature, $1000/T$, on the water saturated reservoir carbonate. One notes an activated process, with a measured activation energy of 1.9 kcal/mol.

TABLE 3: Variation of T_2 of Water Saturating the Reservoir Carbonate

temp °C	T_2 peak (ms)	temp °C	T_2 peak (ms)
26	87	75	122
38	92	89	142
52	101	96	153

In practice, the longitudinal or transverse relaxation times T_1 or T_2 should be shifted according to

$$T_{1,2}^{r} = T_{1,2}^{l} \exp\left(-\frac{\Delta E}{R}\left(\frac{1}{T_r} - \frac{1}{T_l}\right)\right) \quad (6)$$

Equation 6 is directly derived from eq 3. Here, the supscripts r and l designate the relaxation time measured in the reservoir and the laboratory, respectively. T_l and T_r are the laboratory and reservoir temperature, respectively. ΔE depends on the nature of the rock surface and the fluids considered. Table 4 might be used to estimate orders of magnitude when no data are available. Because of the extreme variety of rock surface, it is however recommended to test the temperature effect for each facies or rock type. The temperature shift in eq 6 is in particular valid for the cutoff relaxation time used to derive irreducible water saturation from T_2 relaxation time distributions measured at 100% water saturation.[1]

V. Conclusion

On the basis of the temperature dependence of NMR relaxation times and a theoretical description of the solid−liquid interactions occurring at the pore surface, we have evidenced the dependence of surface relaxivity upon temperature. The key parameter is the difference of activation energy between the binding energy of molecules at the pore surface and the usual energy associated with the individual molecular diffusing jumps. For water on silica surfaces, the binding energy is large and the temperature dependence of the relaxation times is anomalous, that is to say, decrease with increasing temperature. On the other hand, relaxation times of oil in pores with silica surfaces increase with temperature. For water or oil on calcium carbonate surfaces, the binding energy is weaker and the relaxation times increase with increasing temperature for both fluids. These behaviors were observed on model porous media as well as natural rocks. The study presented here can be used as guidelines to compare NMR well logging data acquired at elevated temperature and laboratory experiments performed at room temperature.

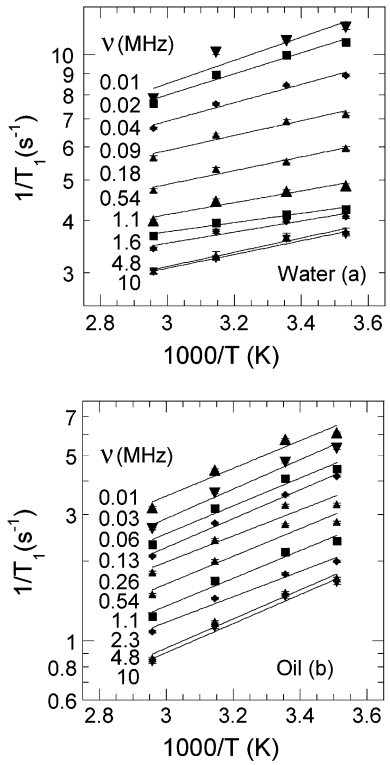

Figure 12. Arrhenius diagrams of the measured relaxation rates of liquids saturating a reservoir carbonate of intermediate wettability(Iw = +0.50), as a function of the inverse of temperature, $1000/T$, for different proton Larmor frequencies, ν, (a) for water and (b) for oil.

TABLE 4: Resume of the Measured Effective Activation Energies, of Water and Oil (Dodecane) in Bulk, or Saturating the Different Porous Media

material	water ΔE kcal/mol	oil ΔE kcal/mol
bulk liquid	4.5	2.6
SiC grain packing	−2	2
calcite grain packing	1.9	
Clashash sandstone	−2	
reservoir sandstone	−1.7	1.5
Lavoux limestone	2.5	
reservoir carbonate	1.9	2.4

Appendix: NMR Cell for Measurements at Elevated Temperature

A special cell was build for the benchtop NMR apparatus used for the measurements at a fixed frequency of 2.2 MHz (MARAN 2 ULTRA equipped with a 51 mm water cooled 1D gradient probe from Resonance Instruments). It allows us to perform experiments at a constant temperature varying from

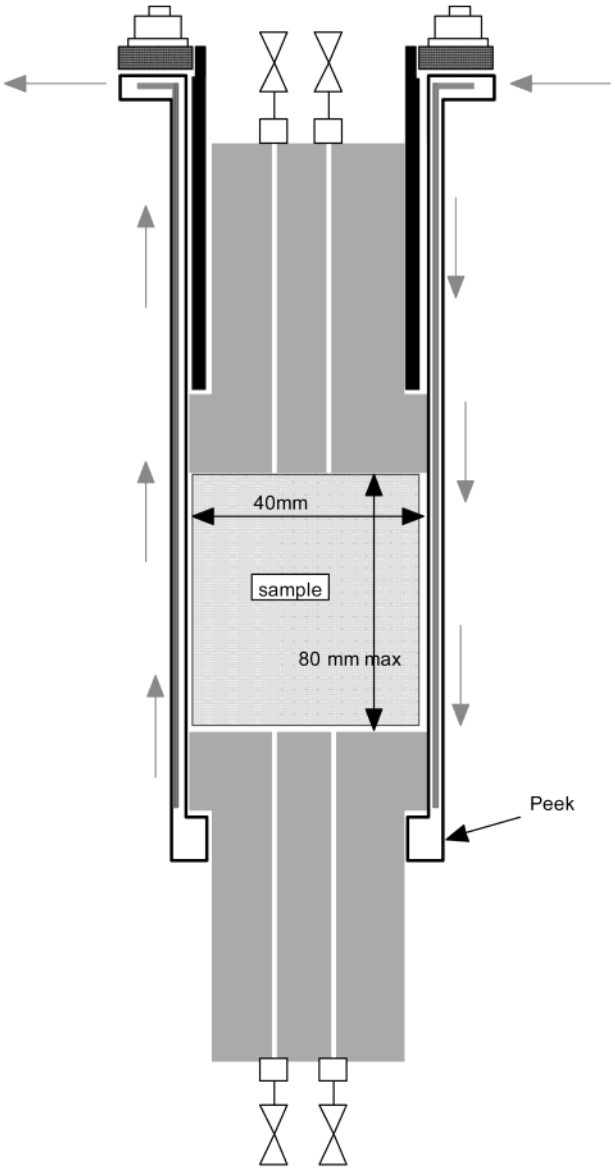

Figure 13. Temperature regulated NMR cell (IFP design) for measuring NMR properties at various temperatures (from 10 up to 100 °C). The outer diameter of the cell is 51 mm. A maximum pressure of 10 bar can be applied to prevent degassing or boiling of the saturating liquid. The optimum length of the sample is 60 mm.

10 up to 100 °C. A small and constant pressure (7 Bar) is maintained inside the cell to prevent degassing or boiling of the saturating liquids. The cell is made of two thin concentric tubes build in Peek (Figure 13) in which a non-hydrogen-liquid (Fluorinert FC43) is circulating. The temperature of this liquid is maintained at a constant temperature using an external bath. At elevated temperature, the heat losses of the cell are evacuated by (i) the water regulation around the antenna (room temperature of about 22 °C) and (ii) the air regulation of the magnet (30 °C).

The experiments were performed on samples with an optimum diameter and length of 40 and 60 mm, respectively. The volume of liquid present between the sample and the cell inner tube is minimized by using a Teflon tape wrapped around the sample. Therefore, there is little perturbation of the sample signal coming from the bulk relaxation of this liquid. Another characteristic of interest is the NMR signal measured on the empty cell. If interpreted as a volume, this signal represents a total of 0.55 cm^3. The relaxation time of the cell material lies at around 0.2 ms and can be detected only with very short echo spacing and a large number of scans. It has no influence in the present experiments.

The temperature of the sample is known from a calibration curve established with a water filled cell and for various bath temperature. From these tests, the stabilization time (about 1 h) was also determined, as well as the accuracy of the temperature regulation (estimated to ± 1 °C). The design of the cell allows performing the long temperature stabilization periods outside the NMR apparatus. When ready, the cell can be placed in the NMR apparatus to proceed with the relaxation measurements.

Acknowledgment. The authors gratefully thank Pr. R. G. Bryant (University of Virginia, Charlotteville) for his participation in the project and Drs. D. Petit and P. Levitz (École Polytechnique, France) and Dr. G. Chauveteau (IFP, France) for stimulating discussions.

References and Notes

(1) Kleinberg, R. L. In *Nuclear Magnetic resonance, Experimental methods in the Physics Sciences: Methods of the physics of the porous media*; Wong, P.-Z., Ed.; 1999.

(2) Kleinberg, R. L. *Encyclopedia of nuclear magnetic resonance*; John Wyley and Sons: New York, 1996; Vol. 6, p 4960.

(3) Latour, L. L; Kleinberg, R. L.; Sezginer, A. *J. Colloid Interface Sci.* **1992**, *150*, 535.

(4) Godefroy, S.; Korb, J.-P.; Fleury, M.; Bryant, R. G. *Phys. Rev. E* **2001**, *64*, 021605.

(5) Abragam, A. *Principles of Nuclear Magnetism*; Clarendon Press: Oxford, U.K., 1961.

(6) Foley, I.; Farooqui, S. A.; Kleinberg, R. L. *J. Magn. Reson. Ser. A* **1996**, *123*, 95.

(7) Cuiec, L. E. *Evaluation of reservoir wettability and its effects on oil recovery*; Morrow, N. R., Ed.; Surfactant Science Series, 36; *Interfacial phenomena in petroleum recovery*.

(8) Korringa, J.; Seevers, D. O.; Torrey, H. C. *Phys. Rev.* **1962**, *127*, 4.

(9) Kleinberg, R. L.; Kenyon, W. E.; Mitra, P. P *J. Magn. Reson. Ser. A* **1994**, *108*, 206.

(10) Korb, J.-P.; Whaley-Hodges, M.; Bryant, R. G. *Phys. Rev. E* **1997**, *56*, 1934.

(11) Korb, J.-P.; Whaley Hodges, M.; Gobron, Th.; Bryant, R. G. *Phys. Rev. E* **1999**, *60*, 3097

(12) Redfield, A. G.; Fite, W.; Bleich, H. E. *Rev. Sci. Instrum.* **1968**, *39*, 710.

(13) Butler, J. P.; Reeds, J. A.; Dawson, S. V. *SIAM J. Numer. Anal.* **1981**, *18*, 381.

(14) Médout-Marère, V.; El Ghzaoui, A.; Charnay, C.; Douillard, J. M.; Chauveteau, G.; Partyka, S. *J. Colloid Interface Sci.* **2000**, *223*, 205.

(15) Dullien, F. A. L. *Porous media, Fluid transport and pore structure*; Academic Press: San Diego, 1992.